Association Aéronautique et Astronautique de France

*56th 3AF International Conference on Applied Aerodynamics*
*28 — 30 March 2022, Toulouse – France*

**FP27-AERO2022-viollet**

# Effect of sharp edges on the unsteady flow and aerodynamic performances of a Boxfish, towards bio-inspired low-drag bluff bodies

**R. Vazquez Casique, M.L. Viollet, M. Bauerheim, V. Chapin and E. Gowree** [(1)]
[(1)] *ISAE-SUPAERO/DAEP, Toulouse, France,* Erwin-ricky.GOWREE@isae-supaero.fr

## ABSTRACT

Several studies have revealed that boxfishes, tropical fishes living in shallow waters, show exceptional aerodynamic performances despite their large volume and cross-sectional area. These characteristics make the boxfish shape an interesting topic of study for drag optimisation of bluff bodies. This study focuses on the aerodynamic analysis of several mathematical shape representations of the boxfish. The effect of the edges is studied since they are responsible for the generation of vortices, which play a role in potentially manipulating the wake, resulting in an overall decrease in the drag coefficient. The effect of the sharpness or roundness of the edges on the aerodynamic performance is investigated. Aerodynamic coefficients are obtained numerically and experimentally for a range of Reynolds numbers between 3000 and 300000 and at pitch angle from $-16^\circ$ to $+20^\circ$.

## 1. INTRODUCTION

In nature, animals and plants have adapted over years of evolution to their environment in order to carry out efficiently the tasks they require for survival. Bio-mimetics and bio-inspired optimisation consist of taking nature as an example of optimal performance for diverse applications. Researchers are trying to transpose some of the remarkable characteristics of natural systems into human-built systems to achieve the same efficiency observed in nature. Such an example is observed in the Boxfish (Teleostei: Ostraciidae), a tropical species of fish living in shallow waters around coral reefs, recognisable by their rigid, bony, and often geometrically shaped carapaces. A very common boxfish, Ostracion cubicus, is displayed in Fig. 1.

Studies have shown that they are very stable and are able to swim on remarkably straight paths through the highly perturbed flow conditions present in coral reefs [5]. Other studies have also shown that they can still exhibit high manoeuvrability despite their rigid carapaces, unlike other species of fishes [10]. Another important characteristic of the boxfish is its low drag coefficient despite being a bluff body with an aspect ratio close to 1/3. The boxfish's large volume and cross-sectional area coupled with their low drag coefficient would allow transport vehicles to transport payload at low drag, reducing fuel cost but more importantly emissions.

Figure 1: Ostracion cubicus [9]

The dynamics of a swimming boxfish was studied by Gordon et al. [6]. In the study, the idea that the boxfish is handling dynamically the flow by using its fins but, more importantly, its body, to generate vortices and almost perfectly balance by continuously adapting its hydrodynamic forces and moments was presented. This work led to further studies on the effect of the body on the stability of the Boxfish. The role of the carapace of the boxfish on stability and maneuverability was investigated by Bartol et. al. [2, 3] through an analysis of the pitch and yaw control. Force balance and Digital Particle Image Velocimetry (DPIV) measurements were used to characterise the performance of the Boxfish. Results showed that the vortices generated near the anterior edges of the ventro-lateral keels grow in strength as they move to the posterior edge of the body. These regions of high vorticity generate a suction effect in the

posterior part of the body, which create restoring moments for pitching motions. The vortices and the self-correcting moment have been shown to be directly proportional to the pitch angle of the boxfish. It has been shown that multiple parts of the carapace play important roles in the generation of vorticity [2]. The work was extended to three other species of Boxfish with varying cross-sectional shapes in 2004 [3], for which the results show a similar tendency; the carapace of the Boxfish produces self-trimming and restoring moments through the creation and amplification of vortices in the keels. Studies, carried out with actively swimming Boxfish, have allowed to separate the contribution of the body and the fins, as well as their interactions [4]. The self-correcting flows observed around static carapace models were verified for actively swimming boxfishes, with a higher vorticity and irregular shapes because of the interaction between fin movement and the carapace. The formation of the vortical flows below the ventral keels was validated, and it was found that the self-correcting keel-induced leading edge vortices do not necessarily act in isolation, and can be modified with powered input from the fins [4]. The use of pectoral fin motions allow the Boxfish to improve stability or manoeuvrability as desired. For stability improvement, pectoral fin motions supplement the passive self-correcting control mechanism by powering it with more flow as required. To enhance manoeuvrability, the pectoral fin generates circulatory forces capable of producing vorticity of similar magnitude to that produced by the keels.

The effect of the vortices induced by the carapace of the Boxfish, defined as 'self-stabilising' by Bartol [4], are stated to be too small to have a significant effect by Van Wassenbergh [8]. It is argued that the stabilising moments created by the vortices, posterior of the centre of mass, are negligible compared with the moment caused by the frontal pressure wave on the head during pitch and yaw. This hypothesis is supported by arguing that having a destabilising flow over the boxfish's body is adequate with its swimming style and environment since it promoted manoeuvrability. Numerical results revealed that during pitching, 76% of the stabilising moments are cancelled by destabilising moments. For yawing motion, all stabilising moments are cancelled.

All previous studies found in the literature suggest that the Boxfish shape is interesting to study as it presents enhanced aerodynamic performance and, although contradicting, high manoeuvrability and stability. However, the possible low drag characteristic which potentially enables its relatively non-negligible speed, of similar range as automobiles in terms of body length displacement per second, has not been thoroughly investigated. The work presented aims to characterise the flow around a boxfish shape to understand better the flow characteristics which enable the Boxfish to swim efficiently in its environment. The study focuses on the effect of the Reynolds number on the aerodynamic forces, for Reynolds number ranging from 3000 to 300000, in order to characterise the flow regimes and for comparison with more canonical bluff bodies. To achieve this wide range of Reynolds number both numerical and experimental studies are performed. The effect of pitching is also examined. Finally, a sensitivity of the aerodynamic forces to small but strategic geometrical characteristics of the Boxfish is carried out focusing on sharp edges on the carapace, capable of triggering in-phase vortical structures.

## 2. MATERIAL AND METHOD

### 2.1 Model construction

The boxfish shapes studied here are simplified mathematical geometries that have been slightly modified from a real scanned carapace of an Ostracion Cubicus. This species of boxfish is characterised by its semi-rectangular shape with four edges. The models were made using a scan fitting routine, representing the geometry by a finite collection of points in space, and then fitting a NURBS surface to the points. This allows the models to keep some concavities specific to the real boxfish shape. With this method an aspect ratio of about 1/3 is obtained. The effect of the sharp edges on the aerodynamic performance of the boxfish shape is studied by changing the sharpness or roundness of the edges. The geometries, presented in Fig. 2, are used for numerical simulations and are modelled to have no sharp edges, two sharp edges, and all four sharp edges, denominated BV0, BV2, and BV4, respectively. An experimental campaign was also carried out for the BV4 shape. The length of the boxfish is the reference length used to compute the Reynolds number. For both numerical and experimental analysis, the angle of incidence, $\alpha$, refers to the angle between the free-stream flow and the centreline of the fish derived from the CAD drawing. On Fig. 2, the boxfish shapes are presented at $\alpha = 0^{\circ}$.

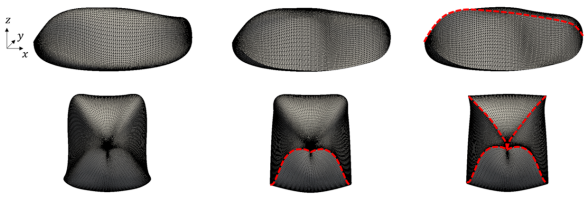

Figure 2: Simplified boxfish geometries: BV0 (left), BV2 (centre), and BV4 (right). Red edges signify edges which are modelled as sharp.

## 2.2 Numerical Analysis

A Lattice-Boltzmann Methods (LBM) solver is used to carry out Direct Numerical Simulations (DNS) at several Reynolds numbers. Based on the length of the boxfish shape, Reynolds number from 3000 to 105000 have been investigated. Simulation settings are set to an upstream velocity of 1 $m/s$, a characteristic length of 1 $m$, and air density of 1 $kg/m^3$. The Reynolds number is varied by changing the value of the kinematic viscosity. Simulations are carried out at a Reynolds number of 3000 for BV0, BV2 and BV4 for positive $\alpha$ values of 0°, 5°, 10°, 15° and 20°. Simulations on BV4 with no pitch have also been carried out for Reynolds numbers of 10000, 20000, 35000, 50000, 65000, and 105000.

The mesh is based on an octree structure, which allows cutting the domain into several cubic regions with different levels of refinement. The geometries and the wake are positioned in the highest level of refinement, to capture with accuracy the relevant flow characteristics. The rectangular domain has dimensions of 37.5 $m$ in the x-direction, 30 $m$ in the y-direction, and 30 $m$ in the z-direction. A mesh independence study was carried out to determine the best compromise between computational cost and accuracy. To this effect, first it was carried out for a canonical flow around a sphere at a Reynolds number of 3000, based on the sphere diameter, for which validation data exist. Three different meshes, from M1 to M3, with different levels of refinement were simulated, and the results are shown in Table 1. Based on these results, M2 was chosen as it is able to reliably predict the expected drag coefficient at this Reynolds number and provide enough refinement at the lowest level to discretise with enough points the geometry without increasing the computational cost of the simulations. An unsteady analysis of the forces obtained by LBM show that for M2, the correct Strouhal numbers were captured in agreement with the results obtained by Yun et al [1]. A Strouhal number of 1, related to the vortex shedding of the sphere, and the correct mean drag coefficient of approximately 0.4 were obtained.

Simulations with the 3 meshes were carried out on BV4 to validate the mesh choice. The results, presented in Table 2, confirm that the choice of M2 for simulation on the BV shapes will allow a good trade-off between precision and cost of simulation.

As the flow behind the boxfish is expected to be unsteady, a time independence study was also carried out.

| Mesh | mean ($C_D$) |
|---|---|
| M1 | 0.4126 (+0.56%) |
| M2 | 0.4152 (+1.1%) |
| M3 | 0.4107 |

Table 2: Mesh independence study on BV4

Three different time steps were investigated, $dt = dx \cdot 10^{-1}$, $dt = 2dx \cdot 10^{-1}$ and $dt = 3dx \cdot 10^{-1}$. This time independent study was performed using M1 to reduce the computational cost. The results, presented in Table 3, show very close results between the drag coefficient for all time steps. It was decided to keep T1 as it will allow to save computational time and it has shown that it is capable of capturing accurately both the steady and the unsteady flow over the sphere.

| | $dt$ | mean ($C_D$) |
|---|---|---|
| T1 | $1.46 \cdot 10^{-3}$ | 0.4126 |
| T2 | $2.92 \cdot 10^{-3}$ | 0.4077 (+1.1%) |
| T3 | $4.39 \cdot 10^{-3}$ | 0.4132 (+0.1%) |

Table 3: Time independence study on BV4

## 2.3 Wind tunnel measurements

Force measurements have been conducted at ISAE-Supaero's subsonic wind tunnel on a 3D printed BV4 model in order to obtain the drag and lift. The printed BV4 shape was post-treated manually to remove unwanted surface imperfections to avoid tripping the boundary layer. The model has a body length of 160 mm, resulting in a reference cross-sectional area of $A_{ref} = 0.00337\ m^2$. The wind tunnel has a 65 $cm$ long test section with a cross-sectional area of 45 $x$ 45 $cm$, resulting in a blockage ratio of 1.66% at 0° pitch angle. The wind tunnel had stable flow range for velocities between 6 $m/s$ (= 37 Body Lengths/s) and 28 $m/s$ (= 175 Body Lengths/s), therefore the Reynolds number of 65000 and 300000 could be achieved.

The model is mounted on top of an in-house force balance thanks to three streamlined and tapered supports, shown in Fig. 3. The assembly allows to pitch the model from $-16°$ to $+20°$ from the geometric angle. The calibration of the balance was done at the beginning of the test campaign with weights in the range of

Table 1: Mesh independence study

| Mesh | Points on the chord | dx at finest level | dt at finest level | lattice nodes | mean ($C_D$) |
|---|---|---|---|---|---|
| M1 | 68 | 0.0146 | 0.00146 | 4551680 | 0.409 |
| M2 | 137 | 0.0073 | 0.00073 | 36413440 | 0.401 |
| M3 | 204 | 0.0049 | 0.00049 | 86676480 | 0.400 |

the expected forces produced by the model in the direction of lift and drag. The contribution of the 3 stands on the measured forces are not negligible, therefore off-wind and on-wind measurements have been undertaken to subtract their contribution on the force measurements during post processing. The force coefficients are then computed as such: $C_l = (2 \cdot L)/(\rho \cdot V^2 \cdot A_{ref})$ and $C_d = (2 \cdot D)/(\rho \cdot V^2 \cdot A_{ref})$, with L and D the lift and drag forces acting on the boxfish, respectively.

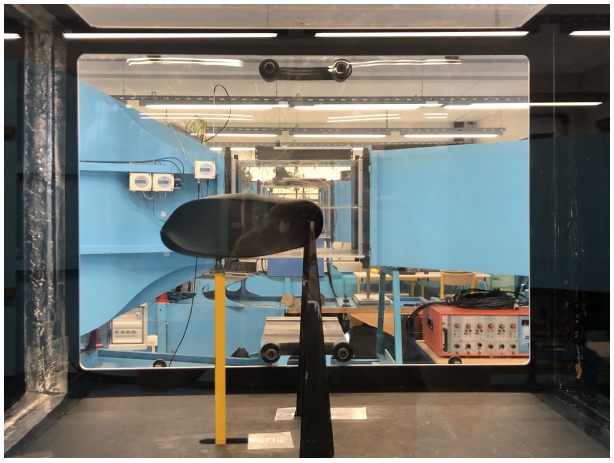

Figure 3: Experimental wind tunnel setup using 3D printed and smoothed BV4 shape.

For each measurement, the output data, such as velocity, drag, and lift are recorded for 10 seconds at a frequency of 10Hz, giving 100 measurements. In the post processing the mean values are presented, with the error bar corresponding to the standard deviation taken during one realisation. The standard deviation was lower than 2% for most of the aerodynamic coefficient measurements.

## 3. RESULTS

### 3.1 Influence of the Reynolds number on the aerodynamic forces

Figure 4 presents numerical and experimental results on the evolution of the drag coefficient as a function of the Reynolds number for the BV4 shape at a 0° pitch angle. It is observed that the drag coefficient is highly dependent on the Reynolds number and that a decrease in the drag coefficient is observed with an increasing Reynolds number. We observe a mismatch in the drag coefficient estimation between the numerical and experimental results at the Reynolds numbers of 65000 and 105000.

Previous investigations on the influence of the Reynolds number on the drag coefficient of a boxfish were performed by Van Wassenbergh et al. [8] on an Ostracion Cubicus shape. The results were obtained by

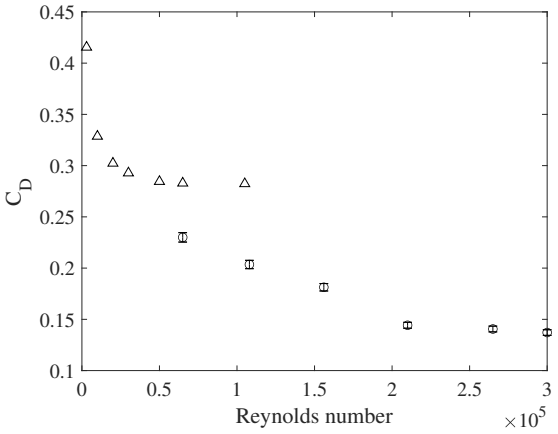


Figure 4: BV4 drag coefficient function of the Reynolds number, from simulations (△) and experiments (○)

measurements in a water tank for Reynolds numbers between 3400 and 68000. It is important to point out that the results obtained by Van Wassenbergh et al. [8] at low Reynolds numbers present high errors and are thus not completely indicative of the drag coefficient of the shape at this range. The results obtained after a Reynolds number of 30000 show a more reliable accuracy and are in a reasonable agreement with respect to simulations carried out. Figure 5 shows that the experimental results obtained in the wind tunnel follow a similar trend as the one observed by Wassenbergh et al. [8]. At the low Reynolds region, around 65000, both numerical and experimental estimations of the drag coefficient are in close range with the results obtained by Wassenbergh et al.[8] and Bartol et al. [3]. A comparison of the average results at a Reynolds number of approximately 65000 can be made in Table 4. The differences found in the results obtained at the various Reynolds numbers compared to those found in literature can in part be attributed to the slight geometric differences of the boxfish shapes studied by Wassenbergh et al. [8] and Bartol et al. [3] with respect to BV4. The tendency, however, shows that the boxfish shape does not present a sudden drag crisis as other bluff bodies, like the sphere or the ellipsoid represented in Fig. 5. Instead, it shows a slower decrease in the drag coefficient with increase of the Reynolds number. The presented drag coefficient is for an ellipsoid with an aspect ratio of 1:1.8 [7]. As expected, due to the more streamlined geometry of an ellipsoid at an aspect ratio of 1:1.8, the drag coefficient of the ellipsoid is lower than the drag of the boxfish. This puts the boxfish shape in a region between the drag coefficient of the sphere and of an ellipsoid.

To see if a different regime can be triggered an experiment to trip the boundary layer of the boxfish has been performed. A trip is added on the 4 faces of the body at a chord-wise length x/c = 0.38 shown in Fig. 6, in order to force the transition of the boundary layer to delay the

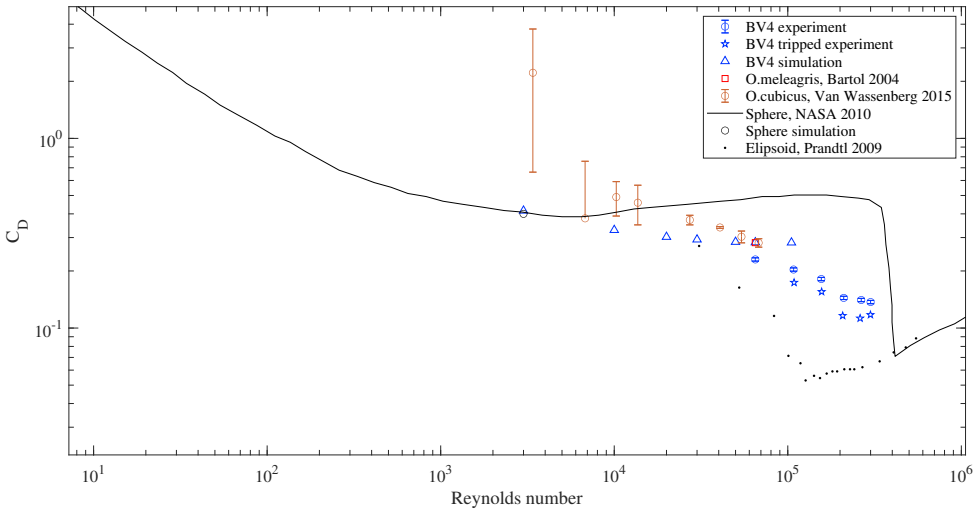


Figure 5: Drag coefficient of several geometries considered as bluff bodies as a function of Reynolds numbers.

| **Author** | boxfish | Re | Cd |
|---|---|---|---|
| Numerical | BV4 | 65 000 | 0.2829 |
| Experiment | BV4 | 65 000 | 0.2300 |
| Van Wassenbergh 2014 [8] | Ostracion cubicus | 68 000 | 0.2814 |
| Bartol 2004 [3] | Ostracion meleagris | 65 000 | 0.282 |

Table 4: Drag coefficient at Re≈65000 for multiple boxfish models.

separation. This usually leads to a decrease in the drag coefficient as the flow stays attached to the body and the major source of drag is due to the separated flow behind bluff bodies. The results of the experiment on BV4 show indeed that when the boundary layer is tripped the drag coefficient is lowered, as observed in Fig. 5. Further flow analysis is needed to better understand this behaviour.

Figure 6: Location of the trip position. Tripping was implemented by employing a sufficiently thin tape wrapped around the shape.

## 3.2 Influence of the angle of incidence on the aerodynamic forces

The lift and drag coefficients are observed to be highly dependent on the angle of attack, as seen in Fig. 7. The lift coefficient is directly proportional to the angle of incidence and shows a similar tendency to that of lifting surfaces. It can be observed that the slope of the curves do not change greatly with varying Reynolds number. At the geometric angle of attack equal to zero, the lift coefficient is approximately zero. Results by Bartol et. al. [3] at Reynolds number of 65000 show a similar trend. It is observed that the slope from Bartol et. al. is slightly lower than the experimental results of this study. This is due to the Reynolds number of used by Bartol et. al. No noticeable stall is observed even at very high pitch angle. This is due to the contribution from the vortices generated by the edges of the boxfish, similar to the leading-edge separation-induced vortex lift generated on delta wings. These vortices were previously reported by Bartol et. al. and were also captured by our current simulation presented in Fig. 12. The rather erratic behaviour in the lift at Re = 65000 is an artefact related to the sensitivity of the balance in detecting and capturing very small loads which were of the order of a couple of grams in this case.

The drag coefficient is highly dependant on the pitch angle. The results obtained through the experimental campaign present a parabolic tendency centered around a geometric incidence angle equal to 0, which is coherent with Bartol et. al. [3] results. The plateau observed between the pitch angles of $-10^\circ$ to $10^\circ$ is respected, and the drag coefficient grows again with pitching angles outside this range. The sharp rise in drag is potentially due to the increasing contribution of the form drag but also the induced drag component resulting from the non-

negligible amount of lift generated with increasing angle of incidence. A difference in the angle at which the minimum drag coefficient is observed exists between the Ostracion meleagris shape [3] and the BV4 shape. It is at $-4°$ for the former while it is situated at $+3°$ for the latter. This difference can be explained by the difference in geometry between the two models (the shape, the definition of the geometric angle and the roughness) and possibly the set-up, where the mounting struts can undergo interaction with the flow.

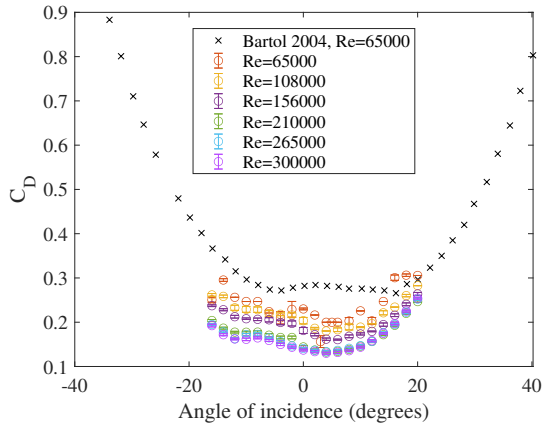


(a) Experimental drag coefficient polar curves for BV4 at varying Reynolds number.

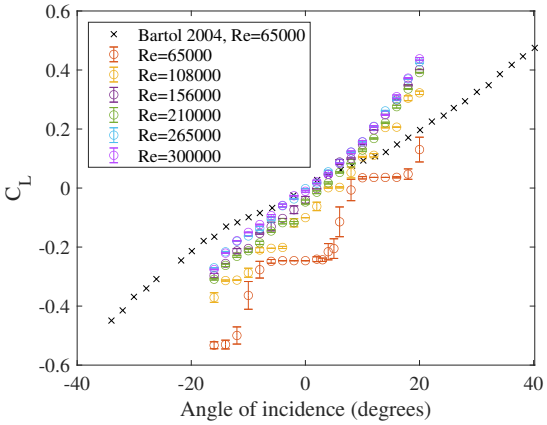


(b) Experimental lift coefficient polar curves for BV4 at varying Reynolds number.

Figure 7: Experimental aerodynamic coefficient polar curves for the BV4 shape at varying Reynolds numbers. Results by [3] presented for comparison.

## 3.3 Effect of the body edges

After building-up some confidence from the numerical simulation capability shown in 5 we proceeded with the analysis of the effect of the edges from the boxfish's body. Numerical simulations were carried out for BV0, BV2, and BV4 at multiple pitch angles at $Re = 3x10e3$ as the cost of simulation could increase drastically considering the total number of cases to be simulated. The evolution of the aerodynamic coefficients with respect to angle of incidence for each shape is presented on Fig. 8. It can be observed that all shapes follow the same trend as seen for higher Reynolds number, i.e. the drag coefficient follows a near parabolic trend and the lift coefficient a linear trend with no stall behaviour was observed. It is interesting to note that the slopes of the lift coefficient evolution are different depending on the shapes, which can explain the difference in slope observed with the results from Bartol et. al. [3] as a real fish was used. In general the tendency in the lift showed strong dependence on the effect of edge modification. For a configuration which mixes both sharp and smooth edges, BV2, the lift coefficient is higher at high angles of attack compared to configurations where all edges are modelled either as smooth or sharp, BV0 and BV4 respectively. At low angles of attack BV0 and BV4 show similar increment in lift, potentially due to the symmetry in terms of edge modifications. However, the difference between these two configurations starts to increase at $\alpha > 15°$. The major difference here in terms of shape is the smoothness of the edges and with sharper edges stronger vortices will be favoured on the BV4 contributing to additional lift. The larger difference from BV2 therefore emanates from a combination of stronger suction in the presence of the edge vortices and also a larger pressure difference promoted by asymmetry in edges.

From the evolution of the drag coefficient as a function of angle of incidence shown in Fig. 8a a similar trend is depicted as that in Fig. 7a for the BV4 measured at significantly higher Reynolds number. Similar to the lift, the drag increased with increasing angle of incidence for all three cases, and once again this is due to a rapid increase in form drag and induced drag due to the rapid increase in lift. However, unlike the lift at very low angle of incidence both modified shapes, BV2 and BV4 showed closer agreement and were slightly higher than the unmodified BV0 case. The presence of sharp edges results in increases in the drag coefficient which can be significant at high incidence angles. The highest drag coefficients are associated to the configuration which combines both sharp and smooth edges, indicating that the disparity in vorticity between shapes results in a high increase of the drag of the shape, compared to shapes which have all edges modelled with the same sharpness. Between BV0 and BV4 the difference in drag only becomes significant at incidence angles around $20°$. From 8, at $0°$ and $5°$ the drag between BV2 and BV4 are closer whereas the lift are similar for all three cases. At $10°$ the drag between BV0 and BV4 remained very close while BV2 experienced a higher drag which increased at a faster rate than BV0 and BV4 except at $\alpha > 15°$. The large difference

arising from BV2 is due to the rapid increase in induced drag in comparison to BV0 and BV4. In this case, the increase is mainly due to the contribution of induced drag which is proportional to the lift coefficient to the square.

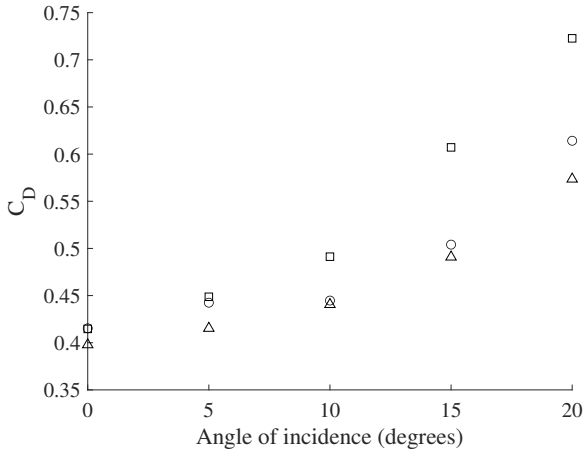


(a) Drag coefficient polar curves for BV4 (○), BV2(□), and BV0 (△) shapes at Reynolds number 3000

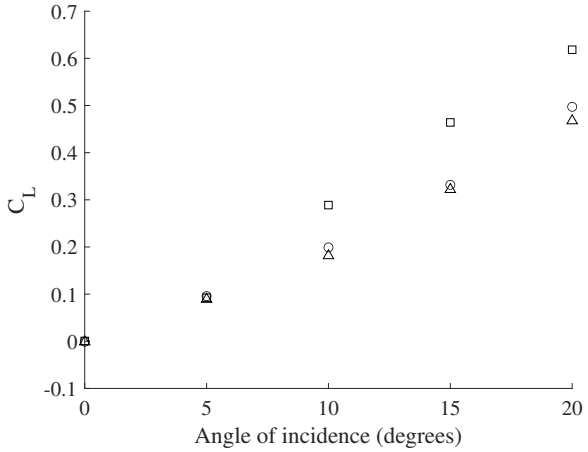


(b) Lift coefficient polar curves for BV4 (○), BV2(□), and BV0 (△) shapes at Reynolds number 3000

Figure 8: Numerical predictions of the aerodynamic coefficients for the BV0, BV2, and BV4 shapes at positive pitch angles.

To further understand the difference in the mean drag results, the time history of the drag coefficient at 0° is plotted on Fig. 9a. A quasi-steady flow can be observed for all shapes, with steady oscillations of seemingly similar frequency in the drag coefficient. An average drag coefficient of approximately 0.415 is obtained for BV2 and BV4, while BV0 shows a lower value of 0.397. A spectral analysis shows that for all shapes two dominating peaks were observed corresponding to two Strouhal numbers of 0.562 and 1.185. Furthermore, it is observed in Fig. 9a that BV2 and BV4 present a higher period oscil-

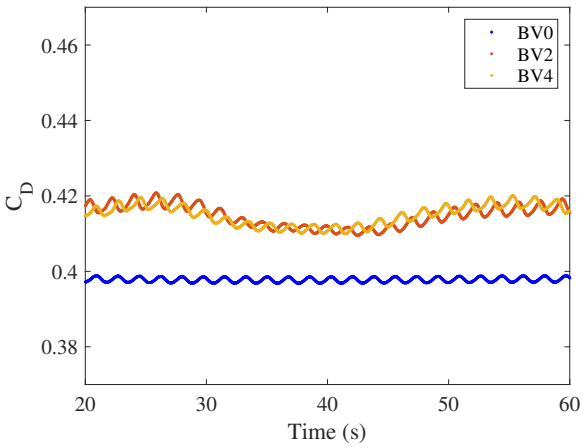


(a) Time history of drag coefficient for BV0 (blue), BV2 (red), and BV4 (yellow) at 0° positive pitch angle and Re=3000.

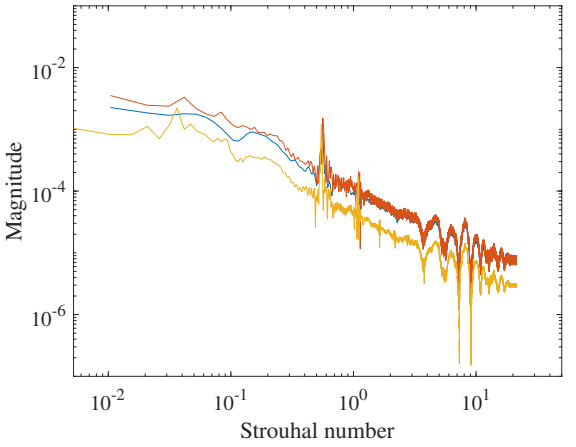


(b) Spectral analysis of the drag coefficient variation for BV0 (blue), BV2 (red), and BV4 (yellow) at 0° positive pitch angle.

Figure 9: Time history of drag coefficient and spectral analysis for all shapes at 0°.

lation corresponding respectively to a Strouhal number of 0.042 and 0.036, which is not observed for BV0. This low Strouhal number is not present in the wake analysis so a possible hypothesis is the existence of low frequency instabilities related to the sharp edges. The existence of the higher Strouhal numbers and their relation to the wake instabilities are supported by findings in other flows around bluff bodies, such as the flow around a sphere, where a Strouhal number of 1 is found at a Reynolds number of 3700 [1].

The flow around the BV0 and in its wake was further analysed. It can be observed in Fig. 10 that four vortices are created at the region corresponding to the eye section (x/L=0.2) of the boxfish as found by Bartol et. al. [3] and Van Wassenbergh et. al. [8]. Much smaller vortices are also formed at the mid height at this section

(x/L=0.2). The vortices are roughly of the same magnitude and counter-rotating between adjacent vortices. They remain attached to the body as they travel downstream. In the wake, at x/L= 1.5, the four vortices are fully developed. The interaction can be observed in the wake between the upper and lower vortices and also between vortices that are side by side.

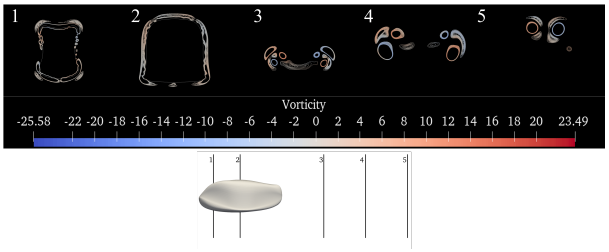


Figure 10: Vorticity along BV0 shape and wake at 0° pitch angle. Cuts (1, 2, 3, 4, 5) at (x/L=0.2, 0.5, 1.5, 2.0, 2.5) from leading-edge.

A preliminary analysis of this phenomenon seems to indicate that the absence of sharp edges on the BV0 shape, compared to BV2 and BV4, results in a slight reduction of the drag coefficient and also in the disappearance in low frequency oscillations of the flow also evident in the time series in Fig. 9a. The highest Strouhal number is related to the dynamics of the convected vortices in the wake, while the lowest Strouhal number present only on BV2 and BV4 can be directly attributed to the presence of sharp edges as BV0 is modelled entirely with smooth edges. The low frequency in BV2 and BV4 is potentially due to stronger interaction between the edge vortices which are of larger magnitude when emanating from a sharp edge as opposed to a rounded one. The propagation of these vortices in the wake and the resulting interaction would thus modify the dynamics of the wake. Further analysis of the unsteady behaviour of the wake should shed some more light on this.

This tendency in the behaviour of the drag coefficient and the dominating Strouhal numbers are maintained until a pitch angle of approximately 10°, where a high increase of the drag coefficient for BV2 is observed. At a pitch angle of 10° the drag coefficient evolution for BV2 seems to reach a stable value with very small oscillations while for BV0 and BV4, the drag coefficient evolution follows slightly more chaotic oscillations, as can be seen on Fig. 11a. BV0 and BV4 seem to result in similar behaviour between the upper and lower regions and thus lower drag coefficients. It is likely that the similarity between the upper and lower edges in the geometries cause vortices which are of similar magnitude and undergo weaker interactions. At high incidence angles, the upper vortices grow in strength to create a self-correcting moment due to the low pressure region associated to them, this is supported by findings in [3] and [8].

At a pitch angle of 10°, the low frequencies are favoured as they increase in amplitude while the peaks observed at 0° at high frequencies are much reduced for all shapes. The peaks from the spectra in Fig. 9a where still present for the case of BV0 and BV4 despite being at significantly lower magnitudes as seen in Fig. 11a, unlike the BV2. Since these peaks are associated with the dynamics of the wake, their gradual elimination with increasing angle of incidence would suggest that they undergo stronger interaction resulting in faster break-down. From Fig. 12 this effect is seen to be more pronounced in BV2 due to the asymmetry in the magnitude of the vortices between the lower and upper surface and thus accelerating the break-down process. Traditionally on bluff bodies a break-down in the wake could result in the reduction of form drag, but here the rapid increase in lift resulting in induced drag makes it difficult to postulate on the form drag.

## 4. SUMMARY

Numerical and experimental wind tunnel studies have been carried out for different boxfish shapes created from mathematical representations and optimisations based on a real Ostracion cubicus specimen. Three shapes with different sharpness or curvature of the edges have been modelled and analysed to evaluate the effect of the edges in the aerodynamic performance of the boxfish shape. Experiments and numerical simulations done for BV4, the shape with all edges modelled as sharp, for a range of Reynolds number showed that the drag coefficient evolution does not show a pronounced drag crisis like observed in other shapes such as a sphere or an ellipsoid. Instead, a smooth decrease in the drag coefficient is observed with increasing Reynolds number. Comparison with the results obtained by Bartol et al. [3] and Van Wassenbergh et al. [8] show that this tendency is expected for similar boxfish shapes.

An analysis of the evolution of the aerodynamic coefficients as a function of positive pitching angle shows that for the angles, up to 20°, there is no stall behaviour on the BV4 shape. This finding is supported by study carried out by Bartol et al. [3]. The drag coefficient evolution with pitch angle follows a near parabolic behaviour. A plateau, where the drag coefficient does not change greatly, is observed for low pitching angles experimentally for BV4.

A numerical analysis on the aerodynamic performance for all shapes at a Reynolds number of 3000 shows that for low incidence angles the shapes present similar drag and lift coefficients regardless of the sharpness or curvature of the edges. At low incidence angles the flow is characterised by the presence of four vortices being formed at the edges of the shapes which grow as they travel downstream. In the wake, the interaction of the system of vortices drives the oscillation of the wake at a

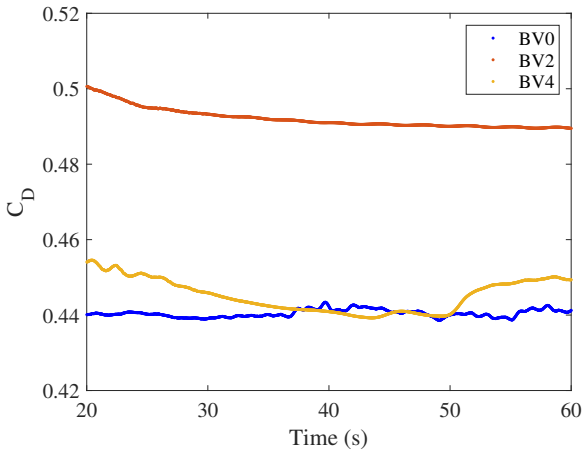


(a) Time history of drag coefficient for BV0 (blue), BV2 (red), and BV4 (yellow) at 10° positive pitch angle and Re=3000.

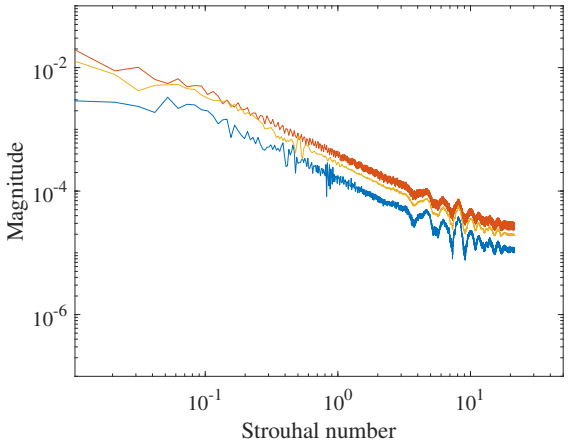


(b) Spectral analysis of the drag coefficient variation for BV0 (blue), BV2 (red), and BV4 (yellow) at 10° positive pitch angle.

Figure 11: Time history of drag coefficient and spectral analysis for all shapes at 10°.

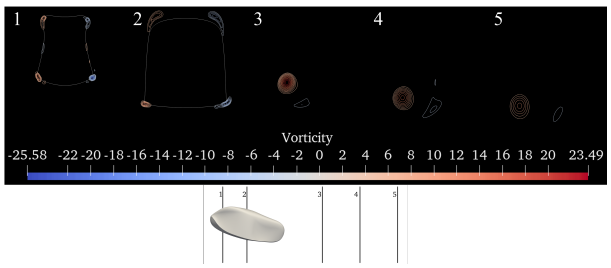


Figure 12: Vorticity along BV2 shape at 10° pitch angle. Cuts (1, 2, 3, 4, 5) at (x/L=0.2, 0.5, 1.5, 2.0, 2.5) from leading-edge.

Strouhal number of 0.562. The vortex shedding between the vortices of the right and the left of the shape occur at two Strouhal numbers of 0.562 and 1.185. At higher pitch angle, starting at 10°, a high increase in the drag coefficient of BV2 is observed. An analysis of the vorticity shows that the upper and the lower being of significantly different magnitudes, while the sharp edge ones being more dominant. This asymmetry in vorticity magnitude affects the dynamics of the wake significantly and potentially provokes an earlier breakdown. Further analysis of the propagation of the edge vortices and their interaction in the wake needs to be conducted both from a steady and an unsteady framework.

## 5. ACKNOWLEDGMENTS

We thank Marc Grellet (ISAE-Supaero) for providing assistance and guidance during the experimental wind tunnel testing campaign carried out. We also thank Sylvain Belliot for his precious help on the coating of the boxfish model use in the experiment.

## REFERENCES

[1] D. Kim G. Yun and H. Choi. Vortical structures behind a sphere at subcritical reynolds numbers. *Physics of Fluids*, 181.

[2] M. Gharib J. Hove P. Webb I. Bartol, M. Gordon and D. Weihs. Flow patterns aroundthe carapaces of rigid-bodied, multi-propulsor boxfishes (teleostei: Ostraciidae). *Integrativeand Comparative Biology*, 42:971–980, 2002.

[3] P. Webb D. Weihs I. Bartol, M. Gharib and M. Gordon. Body-induced vortical flows:a common mechanism for self-corrective trimming control in boxfishes. *The Journal of Experimental Biology*, 208:327–344, 2004.

[4] P. Webb D. Weihs I. Bartol, M. Gordon and M Gharib. Evidence of self-correcting spiral flows in swimming boxfishes. *Bioinspir Biomim*, 2008.

[5] M. Gordon P. Webb J. Hove, L. O'Bryan and D. Weihs. Boxfishes (teleostei: ostracii-dae) as a model system for fishes swimming with many fins: kinematics. *The Journal of Experimental Biology*, 204:1459–1471, 2001.

[6] P. Webb M. Gordon, J. Hove and D. Weihs. Boxfishes as unusually well-controlled autonomous underwater vehicles. *Physiological and Biochemical Zoology: Ecological and Evolutionary Approaches*, 73:663–671, 2000.

[7] L. Prandtl. *Ergebnisse der Aerodynamischen Versuchsanstalt zu Göttingen*. Universitätsverlag Göttingen, 2009.

[8] T. Marcroft M. Alfaro S. Van Wassenbergh, K. van Manen and E. Stamhuis. Boxfish swimming paradox resolved: forces by the flow of water around the body promote manoeuvrability. *J. R. Soc. Interface*, 46, 2014.

[9] Local Dive Thailand. Yellow boxfish – toxic and inspiring?

[10] J. Walker. Does a rigid body limit maneuverability ? *The Journal of Experimental Biology*, 203:3391–3396, 2000.